

THE REDUCTION OF THE ELECTRON ABUNDANCE DURING THE PRE-EXPLOSION SIMMERING IN WHITE DWARF SUPERNOVAE

DAVID A. CHAMULAK^{1,2}, EDWARD F. BROWN^{1,2,3}, F. X. TIMMES^{2,4,5}, AND KIMBERLY DUPCZAK¹

Draft version December 6, 2018

ABSTRACT

Prior to the explosion of a carbon-oxygen white dwarf in a Type Ia supernova there is a long “simmering,” during which the $^{12}\text{C} + ^{12}\text{C}$ reaction gradually heats the white dwarf on a long ($\sim 10^3$ yr) timescale. Piro & Bildsten showed that weak reactions during this simmering set a maximum electron abundance Y_e at the time of the explosion. We investigate the nuclear reactions during this simmering with a series of self-heating, at constant pressure, reaction network calculations. Unlike in AGB stars, proton captures onto ^{22}Ne and heavier trace nuclei do not play a significant role. The ^{12}C abundance is sufficiently high that the neutrons preferentially capture onto ^{12}C , rather than iron group nuclei. As an aid to hydrodynamical simulations of the simmering phase, we present fits to the rates of heating, electron capture, change in mean atomic mass, and consumption of ^{12}C in terms of the screened thermally averaged cross section for $^{12}\text{C} + ^{12}\text{C}$. Our evaluation of the net heating rate includes contributions from electron captures into the 3.68 MeV excited state of ^{13}C . This results in a slightly larger energy release, per ^{12}C consumed, than that found by Piro & Bildsten, but less than that released for a burn to only ^{20}Ne and ^{23}Na . We compare our one-zone results to more accurate integrations over the white dwarf structure to estimate the amount of ^{12}C that must be consumed to raise the white dwarf temperature, and hence to determine the net reduction of Y_e during simmering.

Subject headings: nuclear reactions, nucleosynthesis, abundances — supernovae: general — white dwarfs — galaxies: evolution

1. INTRODUCTION

The leading scenario for a Type Ia supernova (hereafter SNe Ia) is the thermonuclear incineration of a carbon-oxygen white dwarf that has increased in mass, through accretion, to just below the Chandrasekhar limit (for a review, see Hillebrandt & Niemeyer 2000). Despite the advances in modeling the post-ignition flame evolution (for a sampling of recent work, see Gamezo et al. 2004; Plewa et al. 2004; Röpke et al. 2006; Jordan et al. 2007), we still lack a complete understanding of which subset of the binary white dwarf population become SNe Ia, and how differences in the progenitor map onto differences in the outcome of the explosion.

The composition of the white dwarf at the time of the explosion should have an effect on the nucleosynthesis that takes place during the explosion and the isotopic abundances of the final composition. The observable properties of SNe Ia resulting from Chandrasekhar-mass explosions are chiefly determined by their final composition, the velocity profiles of key spectral lines at early- and late-times (e.g., P-Cygni profiles of Si II at 615.0 nm at early times), the opacity of the material through which the photons from radioactive decay must propagate, the kinetic energy of ejecta, and its interaction with the density profile of the surrounding circumstellar or interstellar medium (Filippenko 1997; Pinto & Eastman 2000; Hillebrandt & Niemeyer

2000; Leibundgut 2001; Mazzali & Podsiadlowski 2006; Marion et al. 2006; Blondin et al. 2006; Badenes et al. 2007; Woosley et al. 2007). The dominant parameter in setting the peak brightness, and hence width, of the light curve is widely believed to be the mass of ^{56}Ni ejected by the explosion. Timmes et al. (2003) showed the mass of ^{56}Ni produced depends linearly on the electron fraction, Y_e , at the time of the explosion, and that Y_e itself depends linearly on the abundance of ^{22}Ne in the white dwarf.

In this paper we explore, using a reaction network coupled to an equation for self-heating at constant pressure, the reduction in Y_e that occurs after the onset of the thermonuclear runaway (when the heating from $^{12}\text{C} + ^{12}\text{C}$ reactions is faster than cooling by thermal neutrino emission), but before the burning becomes so fast that local regions can thermally run away and launch a flame. This “simmering” epoch lasts for $\sim 10^3$ yr, long enough that electron captures onto products of ^{12}C burning can reduce the free electron abundance Y_e . A similar, but independent calculation, of the reduction of Y_e during simmering was performed by Piro & Bildsten (2008). Their calculation did not use a full reaction network, but it did take into account the change in energy of the white dwarf due to the growth of the convective zone. Our calculation agrees with their findings, in particular that there is a maximum Y_e at the time of the explosion, and that the reduction in Y_e is linear in the amount of ^{12}C consumed prior to when the rate of ^{12}C burning outpaces that of the weak reactions. This paper expands on their work in three ways. First, by using a full reaction network, we are able to quantify the role of ^{22}Ne and trace nuclides in setting the change in electron abundance with ^{12}C consumption, dY_e/dY_{12} . Second, we calculate the heating from the electron capture reactions and include the contribution from an excited state of ^{13}C . Third, we provide tabulated expressions for the rate of heating ε , the rate of change in electron abundance dY_e/dt , and the rate of change

Electronic address: chamulak@pa.msu.edu

Electronic address: ebrown@pa.msu.edu

Electronic address: fxt44@mac.com

Electronic address: dupczakk@msu.edu

¹ Department of Physics and Astronomy, Michigan State University, East Lansing, MI 48824

² Joint Institute for Nuclear Astrophysics

³ National Superconducting Cyclotron Laboratory

⁴ Thermonuclear Applications, X-2, Los Alamos National Laboratory

⁵ School of Earth and Space Exploration, Arizona State University, Tempe, AZ 85287

in the mean atomic mass $d\langle A \rangle/dt$ in terms of the reaction rate for the $^{12}\text{C} + ^{12}\text{C}$ reaction. These expressions are useful input for large-scale hydrodynamical simulations of the simmering phase which do not resolve such microphysics.

We first give, in § 2, a simple estimate for the reduction in Y_e during the pre-explosion simmering and describe the role of ^{22}Ne and other trace nuclides. In § 3 we describe our numerical calculations, explain the reactive flows that occur (§ 3.1), and give simple approximations to the heating rate and carbon consumption (§ 3.2). We detail, in § 3.3, some of the limitations of our approach. We evaluate the energy required to raise the white dwarf central temperature, and hence the amount of ^{12}C that must be consumed, and compare it against the one-zone calculation. We also estimate the central temperature at which convective mixing becomes faster than electron captures. This convective mixing advects electron capture products to lower densities where they can β^- -decay: the convective Urca process. Because each electron capture-decay cycle emits a neutrino–anti-neutrino pair, there is energy lost from the white dwarf, and our calculation underestimates the amount of ^{12}C consumed prior to the flame runaway. The convective Urca process (Paczynski 1972) reduces the rate of heating by nuclear reactions (thereby increasing the amount of ^{12}C that must be consumed to raise the temperature), but cannot result in a net decrease in entropy and temperature for constant or increasing density (Stein et al. 1999; Stein & Wheeler 2006). The Urca reactions also tend to reduce the effects of buoyancy, and in degenerate matter have a direct influence on the convective velocity (Lesaffre et al. 2005). The paper concludes (§ 4) with a discussion of the implications for systematic variations in the mass of ^{56}Ni produced in the explosion.

2. THE REDUCTION IN ELECTRON ABUNDANCE DURING THE EXPLOSION

The demise of an accreting white dwarf begins when the central temperature and density are such that the heating from the $^{12}\text{C} + ^{12}\text{C}$ reaction becomes greater than the cooling from thermal neutrino emission. For a density $\rho = 2.0 \times 10^9 \text{ g cm}^{-3}$ this requires a temperature $T \approx 3.0 \times 10^8 \text{ K}$ (see Gasques et al. 2005, for a recent calculation). Initially the heating timescale is long, $t_{\text{H}} \equiv T(dT/dt)^{-1} \sim 10^3 \text{ yr}$; as the temperature rises and the reaction rate increases, t_{H} decreases. Woosley et al. (2004) estimate that when $T > 7.6 \times 10^8 \text{ K}$, fluctuations in the temperature are sufficient to ensure that a local patch can run away and the flame ignites.

The basic reactions during ^{12}C burning were first worked out in the context of core carbon burning in evolved stars (Reeves & Salpeter 1959; Cameron 1959). During simmering, ^{12}C is primarily consumed via $^{12}\text{C}(^{12}\text{C}, \alpha)^{20}\text{Ne}$ and $^{12}\text{C}(^{12}\text{C}, p)^{23}\text{Na}$. These reactions occur with a branching ratio 0.56/0.44 for $T < 10^9 \text{ K}$ (Caughlan & Fowler 1988). At temperatures below $\approx 7 \times 10^8 \text{ K}$, neutronization—that is, a reduction in Y_e —occurs via the reaction chain $^{12}\text{C}(p, \gamma)^{13}\text{N}(e^-, \nu_e)^{13}\text{C}$. This electron capture implies that there is a maximum Y_e at the time of the explosion, as first pointed out by Piro & Bildsten (2008). One can readily estimate the change in electron abundance, ΔY_e . For simplicity, take the branching ratio for $^{12}\text{C} + ^{12}\text{C}$ to be 1:1 for producing $p + ^{23}\text{Na}$ and $^4\text{He} + ^{20}\text{Ne}$. Thus there is one p produced for every four ^{12}C consumed. Two additional ^{12}C are consumed via $^{12}\text{C}(n, \gamma)^{13}\text{C}(^4\text{He}, n)^{16}\text{O}$, which also destroys one ^4He nucleus, and via $^{12}\text{C}(p, \gamma)^{13}\text{N}(e^-, \nu_e)^{13}\text{C}$, which also destroys one p . Thus for every 6 ^{12}C consumed there is one electron

capture, so that $dY_e/dY_{12} \approx 1/6$, where Y_{12} is the molar abundance of ^{12}C . As an estimate for the heating from this reaction sequence, summing over the q -values for the strong reactions gives a net heat release of $(16 \text{ MeV})/6 = 2.7 \text{ MeV}$ per ^{12}C nucleus consumed. Note that at densities above $1.7 \times 10^9 \text{ g cm}^{-3}$, the reaction $^{23}\text{Na}(e^-, \nu_e)^{23}\text{Ne}$ contributes to the rate of decrease in Y_e , so that $dY_e/dY_{12} \approx 1/3$ at those densities. The total effective rate of dY_e/dY_{12} depends on the rate of convective mixing and the size of the convective core (see § 3.3) but is always at least as large as the contribution from $^{13}\text{N}(e^-, \nu_e)^{13}\text{C}$. In the following sections, we investigate these reactions in detail.

2.1. The role of neon-22 and other trace nuclides

Reactions on ^{22}Ne , ^{23}Na , and other trace nuclides also occur during shell-burning in asymptotic giant branch (AGB) stars, and we briefly summarize their role in that context before describing the very different environment in a simmering white dwarf core. In AGB stars more massive than about $4 M_{\odot}$, the hydrogen burning shell, at a temperature of 60–100 MK, extends into the convective envelope. The envelope composition is then directly affected by the various hydrogen-burning cycles: CNO, NeNa, and MgAl (Lattanzio & Boothroyd 1997; Herwig 2005). The hydrogen-burning shell is also disturbed by thermal pulses due to ignition of the helium layer. At each pulse, dredge-up of material may occur, in which helium-burnt material is mixed into the stellar envelope, polluting it with ^4He , ^{12}C , ^{22}Ne , and heavy s -process elements (Izzard et al. 2007). Thus, the fate of ^{22}Ne is either to contribute to hydrogen burning via $^{22}\text{Ne}(p, \gamma)^{23}\text{Na}$ or to become a neutron source for the s -process via the $^{22}\text{Ne}(\alpha, n)^{25}\text{Mg}$ reaction. The $^{22}\text{Ne}(\alpha, n)^{25}\text{Mg}$ reaction requires the high temperatures ($T > 2.5 \times 10^8 \text{ K}$) that can be found at the bottom of the pulse-driven convective zone during the helium shell flashes. The neutrons are released with high density [$\log(N_n/\text{cm}^{-3}) \sim 10$] in a short burst (Gallino et al. 1998; Busso et al. 1999). These peak neutron densities are realized for only about a year, followed by a neutron density tail that lasts a few years, depending on the stellar model assumptions. These neutrons are the genesis of the classic high-temperature s -process in AGB stars.

Should ^{23}Na be present, there are two usual possibilities for subsequent nuclear processing in AGB stars via either the $^{23}\text{Na}(p, \alpha)^{20}\text{Ne}$ reaction or the $^{23}\text{Na}(p, \gamma)^{24}\text{Mg}$ reaction. The former reaction gives rise to the classical NeNa cycle (Marion & Fowler 1957; Rolfs & Rodney 1988; Rowland et al. 2004), whereas the competing (p, γ) reaction transforms ^{23}Na to heavier isotopes and bypasses the NeNa cycle. How much material is processed through the (p, α) reaction on ^{23}Na as opposed to the competing (p, γ) reaction is of interest for AGB star (and classical novae) nucleosynthesis. New measurements of the $^{23}\text{Na} + p$ cross section (Rowland et al. 2004) suggest that for $T = (20\text{--}40) \text{ MK}$ $^{23}\text{Na}(p, \gamma)^{24}\text{Mg}$ competes with the (p, α) branch, disrupts the NeNa cycle, and produces a flow into the MgAl hydrogen burning cycle.

Caution about intuition developed for reaction sequences on ^{22}Ne and ^{23}Na in AGB star environments seems prudent when applied to the dense, carbon-rich environments of white dwarfs near the Chandrasekhar mass limit. During the slow ^{12}C simmering preceding the explosion, the large Y_{12} ensures that p liberated by the $^{12}\text{C}(^{12}\text{C}, p)^{23}\text{Na}$ branch will capture preferentially onto ^{12}C , rather than ^{22}Ne or ^{23}Na . Fig-

ure 1 shows the ratio of thermally averaged cross-sections, $\lambda \equiv N_A \langle \sigma v \rangle$, to that for $^{12}\text{C}(p, \gamma)^{13}\text{N}$ for three reactions: $^{22}\text{Ne}(p, \gamma)^{23}\text{Na}$ (solid line), $^{23}\text{Na}(p, \alpha)^{20}\text{Ne}$ (dashed line), and $^{23}\text{Ne}(p, n)^{23}\text{Na}$ (dotted line). In addition to the Coulomb penetration, there are numerous resonances that determine how the cross-sections change with temperature. When the ratio of the thermally averaged cross-sections is of order unity, as it is for $^{22}\text{Ne}(p, \gamma)^{23}\text{Na}$, then the proton capture is determined by the relative abundances of ^{22}Ne and ^{12}C .

Note that for the latter two reactions, we plot the largest proton-consuming branch rather than the (p, γ) branch. We include screening in all reactions (Yakovlev et al. 2006) with the plasma taken to consist of ^{12}C and ^{16}O with mass fraction 0.3 and 0.7, respectively. For $T > 10^8$ K, $\lambda[^{22}\text{Ne}(p, \gamma)^{23}\text{Na}]$ is well-constrained experimentally (Iliadis et al. 2001). For a white dwarf with a central density $\rho = 2 \times 10^9$ g cm $^{-3}$ the ignition temperature (where nuclear heating dominates over cooling via thermal neutrino emission) is $\approx 3 \times 10^8$ K (Gasques et al. 2005); the burning timescale becomes less than the timescale for $^{23}\text{Na}(e^-, \nu_e)^{23}\text{Ne}$ once the temperature increases beyond $T \gtrsim 6 \times 10^8$ K. Over this range, the thermally averaged cross-sections for $^{22}\text{Ne}(p, \gamma)^{23}\text{Na}$ and $^{12}\text{C}(p, \gamma)^{13}\text{N}$ are comparable, but the abundance of ^{12}C is far greater; having p capture preferentially onto ^{22}Ne would therefore require it to have a mass fraction roughly twice that of ^{12}C .

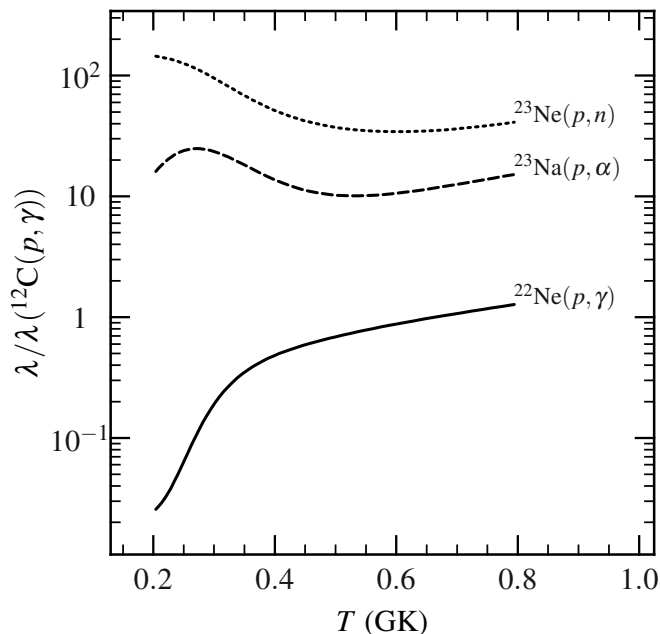


FIG. 1.— Ratio of thermally averaged cross-sections, $\lambda \equiv N_A \langle \sigma v \rangle$, to that for $^{12}\text{C}(p, \gamma)$, for three reactions: $^{22}\text{Ne}(p, \gamma)$ (solid line); $^{23}\text{Na}(p, \alpha)$ (dashed line); and $^{23}\text{Ne}(p, n)$ (dotted line). Screening is included in λ ; we evaluate the ratio at $\rho = 3 \times 10^9$ g cm $^{-3}$ for $^{23}\text{Ne}(p, n)$ and at 10^9 g cm $^{-3}$ for the other two. In the temperature range where the heating timescale is slow enough for weak interactions to reduce Y_e (cf. Fig. 4), the thermally averaged cross-sections for $^{22}\text{Ne}(p, \gamma)$ and $^{12}\text{C}(p, \gamma)$ are of similar magnitude. For ^{22}Ne to compete with ^{12}C for p -captures at $T \gtrsim 3 \times 10^8$ K requires a ^{22}Ne mass fraction $X_{22} \gtrsim (22/12)X_{12}$. At densities less than the electron capture threshold on ^{23}Na a small flow of $^{23}\text{Na}(p, \alpha)^{20}\text{Ne}$ can occur (cf. Fig. 2). At higher densities ^{23}Na electron captures to form ^{23}Ne ; the large cross-section for $^{23}\text{Ne}(p, n)^{23}\text{Na}$ allows it to compete with captures onto ^{12}C if $Y_{23}/Y_{12} \gtrsim 1\%$.

At densities greater than 1.7×10^9 g cm $^{-3}$, the reaction $^{23}\text{Na}(e^-, \nu_e)^{23}\text{Ne}$ produces roughly one ^{23}Ne nucleus for ev-

ery six ^{12}C nuclei consumed. The screened thermally averaged cross-section for $^{23}\text{Ne}(p, n)^{23}\text{Na}$ is $\gtrsim 30$ times that of $^{12}\text{C}(p, \gamma)^{13}\text{N}$ (Fig. 1), so that ^{23}Ne could become a competitive sink for protons. For our self-heating burn (see § 3.1) starting at $\rho = 3 \times 10^9$ g cm $^{-3}$, the abundance of ^{23}Ne reaches $Y_{23} = 3 \times 10^{-4}$ ($Y_{23} \approx 0.015Y_{12}$) by the point the heating timescale τ_H becomes shorter than the timescale for electron captures onto ^{23}Na . Although our one-zone approximation overestimates the amount of ^{12}C that must be consumed to raise the central temperature (see § 3.3), should enough of the convective core lie above the threshold for electron capture onto ^{23}Na , the abundance of ^{23}Ne can become large enough to choke off the $^{12}\text{C}(p, \gamma)^{13}\text{N}$ reaction, as noted by Piro & Bildsten (2008).

2.2. The reaction $^{13}\text{N}(e^-, \nu_e)^{13}\text{C}$

As described above, the large ^{12}C abundance ensures that protons produced by $^{12}\text{C}(p, \gamma)^{13}\text{N}$ lead to the formation of β^+ -unstable ^{13}N via $^{12}\text{C}(p, \gamma)^{13}\text{N}$ unless an appreciable abundance of ^{23}Na or ^{23}Ne can build up. At these densities, the rate for electron capture is substantially greater than the rate of β^+ -decay for ^{13}N . The electron Fermi energy is ≈ 5.1 MeV $(\rho Y_e / 10^9 \text{ g cm}^{-3})^{1/3}$, and the q -value for the β^+ decay of ^{13}N is 2.2 MeV. As a result, there are several excited states of ^{13}C into which the electron can capture. Of these, the transition to the excited state $E_{\text{exc}} = 3.68$ MeV, with spin and parity $J^\pi = 3/2^-$, is an allowed Gamow-Teller transition. We computed the electron capture rate using the experimental $\log ft$ for the ground-state transition (Ajzenberg-Selove 1991). Gamow-Teller strengths to excited states were calculated with the shell-model code OXBASH (Brown et al. 2004) employing the Cohen-Kurath II potential (Cohen & Kurath 1967) in the p -shell model space. A quenching factor of 0.67 (Chou et al. 1993) was applied to this strength, and the resulting ft values were used with the analytical phase space approximations of Becerril Reyes et al. (2006) to obtain the capture rate. These shell-model calculations agree well with recent ($^3\text{He}, t$) scattering data (Zegers et al. 2007). At $\rho Y_e = 10^9$ g cm $^{-3}$, captures into the excited state at $E_{\text{exc}} = 3.68$ MeV account for $\gtrsim 0.3$ of the total rate ($R_{\text{ec}} = 12 \text{ s}^{-1}$); this fraction increases with density. Because $R_{\text{ec}} > (G\bar{\rho})^{-1/2}$, this capture does not freeze out during the simmering, unlike capture onto ^{23}Na . Although the capture into the excited level does not increase the capture rate substantially beyond that for the ground-state-to-ground-state transition, it does increase the heat deposited into the white dwarf from this reaction. We find the heat deposited from this reaction, at $\rho Y_e = 10^9$ g cm $^{-3}$, to be 1.3 MeV.

2.3. Production and subsequent captures of neutrons

Finally, we consider the contribution from heavier nuclei, such as ^{56}Fe , inherited from the main-sequence star. In AGB stars the reaction $^{13}\text{C}(\alpha, n)^{16}\text{O}$ (during a He shell flash, $^{22}\text{Ne}(\alpha, n)^{25}\text{Mg}$ also contributes) acts as a neutron source for the s -process. In contrast, the large ^{12}C abundance of the white dwarf core prevents a strong s -process flow during the pre-explosion simmering. The cross-section for $^{12}\text{C}(n, \gamma)^{13}\text{C}$ is 63.5 times smaller than the cross-section for $^{56}\text{Fe}(n, \gamma)^{57}\text{Fe}$ (Bao & Kappeler 1987) at an energy of 30 MeV, which is not sufficient to overcome the vastly larger abundance of ^{12}C nuclei (for a progenitor with solar metallicity, the $^{12}\text{C} : ^{56}\text{Fe}$ ratio [for a ^{12}C mass fraction of 0.3] is 1400:1).

3. REACTION NETWORK CALCULATIONS

In this section we investigate the reactions that occur during simmering in more detail using a “self-heating” reaction network. Under isobaric conditions the temperature T evolves with time according to

$$\frac{dT}{dt} = \frac{\varepsilon}{C_P}. \quad (1)$$

Here C_P is the specific heat at constant pressure, and the heating rate ε is given by

$$\varepsilon = -N_A \left[c^2 \sum_i \left(M_i \frac{dY_i}{dt} \right) + \mu_e \frac{dY_e}{dt} \right] - \varepsilon_\nu, \quad (2)$$

where M_i and Y_i are, respectively, the atomic mass and molar abundance of species i , μ_e is the electron chemical potential, ε_ν is the neutrino loss rate, per unit mass, from the weak reactions (Fuller et al. 1982; Langanke & Martínez-Pinedo 2001), and $N_A = 6.022 \times 10^{23} \text{ g}^{-1} = (1 \text{ amu})^{-1}$. We neglect thermal neutrino emission processes; this is an excellent approximation over most of the integration. Our reaction network incorporated 430 nuclides up to ${}^{76}\text{Ge}$ and is the same one used to explore the effect of ${}^{22}\text{Ne}$ on the laminar flame speed (see Chamulak et al. 2007, and references therein, for a description of the microphysics). At conditions of $\rho = (1\text{--}3) \times 10^9 \text{ g cm}^{-3}$ and $T = 5 \times 10^8 \text{ K}$, the specific heat C_P is dominated by the ions, which are in a liquid state (plasma parameter $\Gamma \equiv \langle Z^{5/3} \rangle (e^2/k_B T) (\rho Y_e N_A)^{1/3} \approx 10$), and have $C_P \approx 2.9 k_B N_A / \langle A \rangle$, where $\langle A \rangle$ is the average atomic mass.

3.1. The reactive flows

In this section we refine our estimate of dY_e/dY_{12} made in § 2.2. We integrate equations (1)–(2) starting from the temperature at which heating from the ${}^{12}\text{C} + {}^{12}\text{C}$ reaction equals the heat loss from thermal neutrino losses (this determines the onset of thermal instability). For simplicity, we split the solution of the thermal and network equations. That is, for each time-step dt we solve the thermal equations to obtain T and ρ , integrate the reaction network at that T and ρ to compute Y_i and ε , and use ε to advance the solution of equation (1).

In the initial phases of the simmering, the convective timescale is slow, and our one-zone calculations give an adequate description of the heating (when corrected for the gradient in temperature). As the temperature of the white dwarf increases, the heating timescale t_H decreases; moreover, the convective mixing becomes more rapid, and one must treat the hydrodynamical flows in order to calculate the nucleosynthesis properly (see § 3.3). In this section, we will restrict our integration to where $T < 0.6 \text{ GK}$, for which the heating timescale is $\gtrsim 10^4 \text{ s}$, so that electron captures onto ${}^{23}\text{Na}$ are not frozen out.

To explore the reaction channels that link ${}^{12}\text{C}$ consumption with the reduction in Y_e , we define the reactive flow between nuclides i and j as

$$F(i \rightarrow j) \equiv \int_t \left| \frac{dY_i}{dt} \right|_{i \rightarrow j} dt, \quad (3)$$

where the integral is for the reactions linking nuclide i with j . We differentiate between $F(i \rightarrow j)$ and $F(j \rightarrow i)$, i.e., we treat inverse rates separately. Figures 2 and 3 show the reactive flows for $\rho = 10^9 \text{ g cm}^{-3}$ and $3 \times 10^9 \text{ g cm}^{-3}$, respectively. In both cases the composition is $\{X_{12}, X_{16}, X_{22}\} = \{0.3, 0.7, 0.0\}$.

Each row of the chart is a different element (Z), with the columns corresponding to neutron number. For viewing ease, we only plot those flows having $F > 0.01 \cdot \max(F)$, and we indicate the strength of the flow by the line thickness. We highlight the flows of the initial ${}^{12}\text{C}$ fusion reactions with a lighter shading (these flows are also in red in the online version). For illustrative purposes, we only show the flows for when the temperature is not sufficiently hot for photodissociation of ${}^{13}\text{N}$. Finally, by convention and to avoid cluttering the plot, we do not show flows into or out of p , n , and ${}^4\text{He}$.

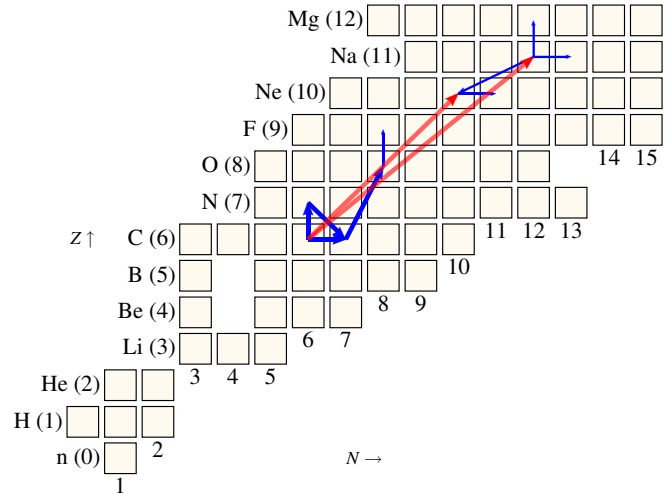


FIG. 2.— Flows during a constant-pressure self-heating burn at $\rho = 10^9 \text{ g cm}^{-3}$ with an initial composition $\{X_{12}, X_{16}, X_{22}\} = \{0.3, 0.7, 0.0\}$. We integrate over the period of the burn with $T < 6 \times 10^8 \text{ K}$. Each row contains the isotopes of a particular element Z , with the columns containing different neutron numbers N . The width of the arrow is proportional to the magnitude of the flow, with only those flows having magnitude $> 0.01 \cdot \max(F)$ being shown. The primary ${}^{12}\text{C} + {}^{12}\text{C}$ reactive flows are indicated with a lighter shading and are in red in the online version.

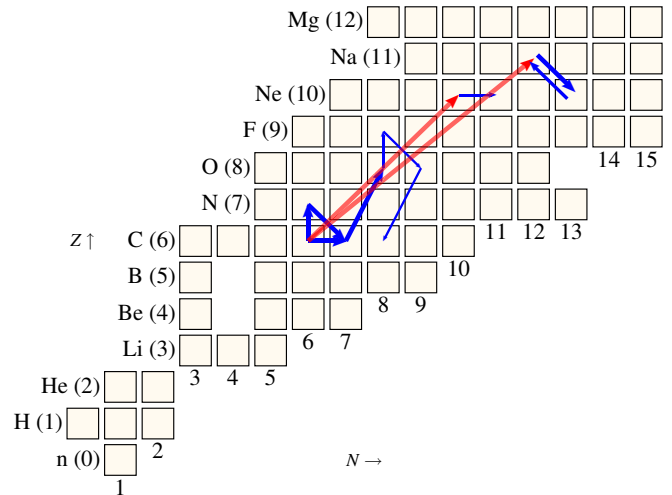


FIG. 3.— Same as in Fig. 2, but at $\rho = 3 \times 10^9 \text{ g cm}^{-3}$. The reaction ${}^{23}\text{Na}(e^-, \nu_e){}^{23}\text{Ne}$ is now the dominant destroyer of ${}^{23}\text{Na}$ instead of (p, α) , and (n, γ) reactions.

To facilitate comparisons between different runs, we define a normalized flow as

$$\tilde{F}(i \rightarrow j) \equiv \frac{F(i \rightarrow j)}{F({}^{12}\text{C} \rightarrow {}^{23}\text{Na}) + F({}^{12}\text{C} \rightarrow {}^{20}\text{Ne})}. \quad (4)$$

At a density of 10^9 g cm^{-3} we find $\tilde{F}(^{12}\text{C} \rightarrow ^{23}\text{Na}) = 0.43$ and $\tilde{F}(^{12}\text{C} \rightarrow ^{20}\text{Ne}) = 0.57$, which reflects the branching ratio (Caughlan & Fowler 1988). In agreement with the arguments in § 2, most of the protons liberated by $^{12}\text{C}(^{12}\text{C}, p)^{23}\text{Na}$ capture onto ^{12}C , with $\tilde{F}(^{12}\text{C} \rightarrow ^{13}\text{N}) \approx \tilde{F}(^{13}\text{N} \rightarrow ^{13}\text{C}) = 0.20$. Note that if all p were to capture onto ^{12}C , we would have $\tilde{F}(^{12}\text{C} \rightarrow ^{13}\text{N})/\tilde{F}(^{12}\text{C} \rightarrow ^{23}\text{Na}) = 0.5$, because the reaction $^{12}\text{C}(^{12}\text{C}, p)^{23}\text{Na}$ consumes two ^{12}C . The α -particle released by the $^{12}\text{C}(^{12}\text{C}, \alpha)^{20}\text{Ne}$ reaction captures onto ^{13}C to form ^{16}O and a neutron, which in turn destroys another ^{12}C via $^{12}\text{C}(n, \gamma)^{13}\text{C}$. The flow $\tilde{F}(^{12}\text{C} \rightarrow ^{13}\text{C}) = 0.26$ and nearly matches the number of α -particles produced by $^{12}\text{C}(^{12}\text{C}, \alpha)^{20}\text{Ne}$; n -captures onto ^{23}Na and ^{20}Ne account for the difference. At $\rho = 10^9 \text{ g cm}^{-3}$ the only electron captures are onto ^{13}N , so $\Delta Y_e = -\tilde{F}(^{13}\text{N} \rightarrow ^{13}\text{C})$. Dividing by $\Delta Y_{12} = -[\tilde{F}(^{12}\text{C} \rightarrow ^{23}\text{Na}) + \tilde{F}(^{12}\text{C} \rightarrow ^{20}\text{Ne}) + \tilde{F}(^{12}\text{C} \rightarrow ^{13}\text{N}) + \tilde{F}(^{12}\text{C} \rightarrow ^{13}\text{C})]$ gives $dY_e/dY_{12} = 0.14$ (Table 1). This is slightly less than the estimate of $1/6$ (§ 2.2) because of the lower branching ratio of $^{12}\text{C} \rightarrow ^{23}\text{Na}$.

At $\rho = 3 \times 10^9 \text{ g cm}^{-3}$, ^{23}Na is consumed by the reaction $^{23}\text{Na}(e^-, \nu_e)^{23}\text{Ne}$ rather than by p - or n -capture (cf. Figs. 2 and 3). The flow is much larger than that from ^{13}N , because the reaction $^{23}\text{Ne}(p, n)^{23}\text{Na}$ competes for p and produces more ^{23}Na . Indeed, $\tilde{F}(^{12}\text{C} \rightarrow ^{13}\text{C}) = 2.5\tilde{F}(^{12}\text{C} \rightarrow ^{13}\text{N})$ because of extra n produced by the reaction $^{23}\text{Ne}(p, n)^{23}\text{Na}$. There is an additional contribution from electron captures onto ^{17}F produced via $^{16}\text{O}(p, \gamma)^{17}\text{F}$, but this flow is only about 4% of the $^{23}\text{Na}(e^-, \nu_e)^{23}\text{Ne}$ flow. At both densities, ^{22}Ne plays a small role in reducing Y_e , which we verified by comparing the flows for a burn with $X_{22} = 0.06$ with those for a flow with $X_{22} = 0.0$ (Fig. 3). We find that, for a burn starting at $\rho = 3.0 \times 10^9 \text{ g cm}^{-3}$, $\tilde{F}(^{22}\text{Ne} \rightarrow ^{23}\text{Na})/\tilde{F}(^{12}\text{C} \rightarrow ^{13}\text{N}) = 0.08$ and $\tilde{F}(^{22}\text{Ne} \rightarrow ^{23}\text{Ne})/\tilde{F}(^{12}\text{C} \rightarrow ^{13}\text{C}) = 0.05$. Although $\lambda[^{22}\text{Ne}(p, \gamma)^{23}\text{Na}] \approx \lambda[^{12}\text{C}(p, \gamma)^{13}\text{N}]$ at $T \lesssim 6 \times 10^8 \text{ K}$ (Fig. 1), the abundances are in ratio $Y_{22}/Y_{12} = 0.11$. Below the electron capture threshold for ^{23}Na , the reaction $^{22}\text{Ne}(p, \gamma)^{23}\text{Na}$ will cause a slight reduction in dY_e/dY_{12} equal to the ratio of $\tilde{F}(^{22}\text{Ne} \rightarrow ^{23}\text{Na})$ to $\tilde{F}(^{12}\text{C} \rightarrow ^{13}\text{N})$.

Finally, we confirmed the lack of an s-process flow (§ 2.3) by performing a run with nuclides from ^{20}Ne to ^{56}Fe present at up to 3 times their solar abundances (Anders & Grevesse 1989). The threshold for electron capture onto ^{56}Fe is $1.5 \times 10^9 \text{ g cm}^{-3}$, and so at higher densities carbon ignition occurs in a more neutron-rich environment. We therefore start the calculation by artificially suppressing the strong interactions and allowing the mixture to come into β -equilibrium. We then turn on the strong reactions and let the runaway commence. In all cases the heavier nuclides did not have a substantial impact on the reactive flows. The value for dY_e/dY_{12} is somewhat larger than 0.3 at densities $\rho \geq 1.2 \times 10^9 \text{ g cm}^{-3}$, the threshold density for $^{25}\text{Mg}(e^-, \nu_e)^{25}\text{Na}(p, n)$, because of the reactions $^{24}\text{Mg}(p, \gamma)^{25}\text{Al}(e^-, \nu_e)^{25}\text{Mg}(e^-, \nu_e)^{25}\text{Na}$. Of these two captures, ^{25}Al is β^+ -unstable, and hence the electron capture is fast enough to proceed throughout simmering; the capture onto ^{25}Mg has a timescale, at $\rho = 2 \times 10^9 \text{ g cm}^{-3}$, of $\approx 900 \text{ s}$ and will therefore freezeout during simmering, just as captures onto ^{23}Na freezeout.

Our runs span a range of initial densities, from 10^9 g cm^{-3} (for which the electron Fermi energy is too low to induce electron captures onto ^{23}Na) to $6 \times 10^9 \text{ g cm}^{-3}$, which represents an extreme case for accretion onto a cold, initially massive white dwarf (Lesaffre et al. 2006). In all cases we took the initial ^{12}C mass fraction to be $X_{12} = 0.3$. As noted above,

TABLE 1
CHANGE IN ELECTRON ABUNDANCE PER CARBON CONSUMED
DURING THE PRE-EXPLOSION CONVECTIVE BURNING

composition ^a	density 10^9 g cm^{-3}	dY_e/dY_{12}	$\sum_i dY_i/dY_{12}$
$X_{22} = 0.00$	1.0	0.136	0.340
...	3.0	0.297	0.340
...	6.0	0.302	0.342
$X_{22} = 0.06$	1.0	0.125	0.347
...	3.0	0.301	0.344
...	6.0	0.305	0.346
$3Z_\odot$	1.0	0.130	0.361
...	3.0	0.349	0.370
...	6.0	0.355	0.380

^a In all cases the initial mass fraction of ^{12}C is 0.3.

the mass fraction of ^{22}Ne would have to exceed that of ^{12}C to change the nucleosynthesis during simmering appreciably. At higher densities, p -captures onto ^{24}Mg can also play a role (§ 3.1), but our results will not change appreciably so long as X_{12} is not substantially less than 0.3.

The calculation, being a single reaction network integration, does not incorporate the effects of mixing in the white dwarf core. Our focus here is to elucidate the reactions that set Y_e . These calculations do not determine the total amount of carbon consumed (although see § 3.3 for an estimate) or the total mass of processed material that lies at a density greater than the electron capture threshold. We list our one-zone results in terms of the change in electron abundance per carbon consumed, dY_e/dY_{12} . Table 1 summarizes our numerical findings of dY_e/dY_{12} for densities 10^9 , 3×10^9 , and $6 \times 10^9 \text{ g cm}^{-3}$, for ^{22}Ne mass fractions $X_{22} = 0$ and 0.06, and finally a run (denoted as $3Z_\odot$ in Table 1) with elements heavier than ^{20}Ne present at 3 times solar abundance. We use this value of $3Z_\odot$ as representing a rough upper limit based on the ≈ 0.5 dex scatter in $[\text{Fe}/\text{H}]$ present in local field stars (Feltzing et al. 2001).

3.2. The effective q -value of the $^{12}\text{C} + ^{12}\text{C}$ reaction

The scope of this work is to elucidate the nuclear reactions that occur during the pre-explosion simmering, and including their effects in large-scale hydrodynamics simulations of the entire white dwarf is advisable. As an aid to such simulations, we present fits for the carbon depletion rate and effective heat deposition, which improve on previous expressions (Woosley et al. 2004). Since the reaction chain is controlled by the reaction $^{12}\text{C} + ^{12}\text{C}$, we write the rate of carbon consumption, dY_{12}/dt as being proportional to the thermally averaged cross-section, $\lambda = N_A \langle \sigma v \rangle$

$$\frac{dY_{12}}{dt} = -M_{12} \left(\frac{1}{2} Y_{12}^2 \rho \lambda \right). \quad (5)$$

This definition is such that the quantity in parenthesis is the reaction rate per pair of ^{12}C nuclei and $M_{12} = 2$ if the only ^{12}C -destroying reaction present is $^{12}\text{C} + ^{12}\text{C}$. One can determine M_{12} from summing the normalized reaction flows (eq. [4]) out of ^{12}C .

In a similar fashion, we can define the effective heat evolved, q_{eff} , per reaction $^{12}\text{C} + ^{12}\text{C}$ by the equation

$$\varepsilon = q_{\text{eff}} N_A \left(\frac{1}{2} Y_{12}^2 \rho \lambda \right). \quad (6)$$

With this definition, one has $\varepsilon = (q_{\text{eff}} N_A / M_{12}) \times dY_{12}/dt$;

this may be compared with equation (2) to relate q_{eff} to the binding energy of the nuclei. To compute these quantities, we integrated the reaction network over a grid of ρ and T , both of which were held fixed for each run. We found in all cases that the instantaneous energy generation rate ε would, after some initial transient fluctuations, settle onto a constant value until a significant ($> 10\%$) depletion in ^{12}C had occurred. We used this plateau in ε to obtain q_{eff} and M_{12} . For the densities of interest, the values of both q_{eff} and M_{12} obtained this way are nearly independent of temperature. We find $M_{12} = 2.93$; this value is accurate to within 2% over all our runs. The value of q_{eff} increases slightly with density, but is nearly constant over the temperature range of interest. We find that $q_{\text{eff}} = 8.91$ MeV, 9.11 MeV, and 9.43 MeV for $\rho = 10^9$ g cm $^{-3}$, 2×10^9 g cm $^{-3}$, and 3×10^9 g cm $^{-3}$, respectively. At each of these densities, the quoted value of q_{eff} is accurate to within 3% over the temperature range of 3×10^8 K to 7×10^8 K.

For use in large-scale hydrodynamic models, one first computes the screened thermally averaged cross-section λ (for the most recent rate, see Gasques et al. 2005) at the thermodynamic conditions of a given cell. Combining λ and the cell's carbon abundance Y_{12} with our estimates of M_{12} and q_{eff} , one computes dY_{12}/dt and ε from equations (5) and (6). In effect, this procedure incorporates the results of a large reaction network and careful treatment of the detailed nuclear physics into simple expressions. We caution that these fits were obtained in the regime $-\Delta Y_{12} < 0.003$, for which proton captures onto ^{23}Na are not competitive with proton captures onto ^{12}C . Note that the heat released per ^{12}C nucleus consumed is $q_{\text{eff}}/M_{12} \approx 3.1$ MeV, slightly higher than our simple estimate (§ 2), and also somewhat higher than those used by Piro & Bildsten (2008). This is because of our inclusion of heating from the $^{13}\text{N}(e^-, \nu_e)^{13}\text{C}$ and $^{23}\text{Na}(e^-, \nu_e)^{23}\text{Ne}$ reactions. Our estimate of the heat evolved is less than that computed under the assumption that the products of ^{12}C burning are a 3:1 $^{20}\text{Ne}:$ ^{24}Mg mixture (see, e.g. Woosley et al. 2004), which releases 5.0 MeV per ^{12}C nucleus consumed⁶. Our net heating rate, per $^{12}\text{C} + ^{12}\text{C}$ reaction, is about 10% less than that used by Woosley et al. (2004), but we effectively consume ≈ 3 ^{12}C nuclei per reaction.

The change in electron abundance is related to λ via

$$\frac{dY_e}{dt} = - \left(M_{12} \frac{dY_e}{dY_{12}} \right) \times \left(\frac{1}{2} Y_{12}^2 \rho \lambda \right), \quad (7)$$

where dY_e/dY_{12} is taken from Table 1. Finally, we may compute the change in the mean atomic mass, $\langle A \rangle$, as a function of carbon consumed. On differentiating $\langle A \rangle = (\sum_i dY_i/dY_{12})^{-1}$, and substituting equation (5), we have

$$\frac{d\langle A \rangle}{dt} = \langle A \rangle^2 M_{12} \left(\frac{1}{2} Y_{12}^2 \rho \lambda \right) \left(\sum_i \frac{dY_i}{dY_{12}} \right), \quad (8)$$

where the quantity $\sum_i dY_i/dY_{12}$ is computed from the flows (eq. [4]) and is listed in Table 1. From the simple description of the reactions (§ 2; see also Piro & Bildsten 2008) we have, for every six ^{12}C destroyed, one each of ^{13}C , ^{16}O , ^{20}Ne , and ^{23}Na (or ^{23}Ne), so that $\sum_i dY_i/dY_{12} \approx \frac{1}{3}$. This results in a smaller change in $\langle A \rangle$ than would result from burning $^{12}\text{C} + ^{12}\text{C}$ to a 3:1 $^{20}\text{Ne}:$ ^{23}Na mixture (in that case, $\sum_i dY_i/dY_{12} =$

⁶ Note that in eq. (1) of Woosley et al. (2004), the factor of $\frac{1}{2}$ is subsumed into their quantity $\lambda_{12,12}$.

0.42). We advocate using equations (5)–(8) and the computed values (Table 1) of dY_e/dY_{12} and $\sum_i dY_i/dY_{12}$ in numerical simulations of simmering.

3.3. Heating of the white dwarf core and the end of simmering

In previous sections, we evaluated the heating and neutronization of the white dwarf core in terms of the rate of ^{12}C consumption. We now estimate the net amount of ^{12}C that is consumed in raising the white dwarf temperature and evaluate the temperature at which electron captures onto ^{23}Na freeze out. In the one-zone isobaric calculations, using equations (5) and (6), we have $dT/dY_{12} = (q_{\text{eff}} N_A)/(M_{12} C_P)$, so that $\Delta T \approx 0.15$ GK ($\Delta X_{12}/0.01$), where ΔX_{12} is the change in mass fraction of ^{12}C . The change of ^{12}C abundance required to raise the temperature from 3×10^8 K to 8×10^8 K is then $|\Delta Y_{12}| \approx 2.8 \times 10^{-3}$. This is about 11% of the available ^{12}C , for an initial ^{12}C mass fraction $X_{12} = 0.3$. Figure 4 shows the decrement of the e^- abundance, $Y_e(t=0) - Y_e(t) = -\Delta Y_e$ as a function of ^{12}C consumed, $Y_{12}(t=0) - Y_{12}(t) = -\Delta Y_{12}$. Note that we are plotting the decrement in abundance. The calculation was started at an initial density and temperature $\rho = 3.0 \times 10^9$ g cm $^{-3}$ and $T = 1.9 \times 10^8$ K. As t_{H} shortens, the electron captures onto ^{23}Na “freeze out” and dY_e/dY_{12} decrease to $\approx 1/6$. When $-\Delta Y_{12} \gtrsim 0.003$, the abundances of ^{23}Na and ^{23}Ne have increased sufficiently that they compete with ^{12}C to consume protons, and thereby halt the neutronization, in agreement with Piro & Bildsten (2008).

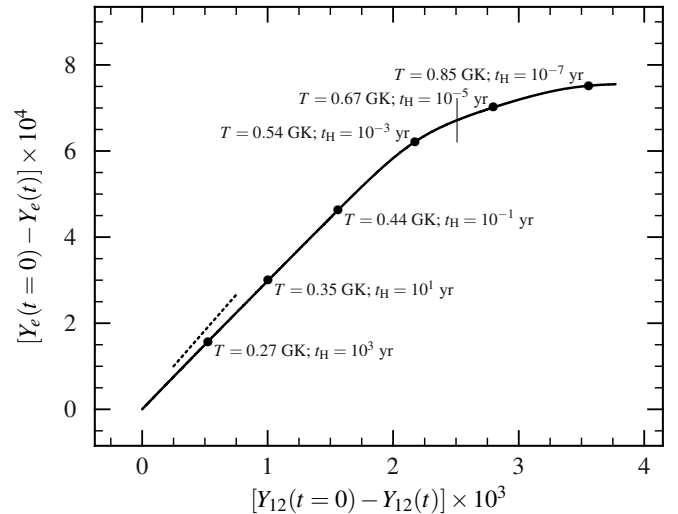


FIG. 4.— Change in electron abundance, $Y_e(t=0) - Y_e(t)$, as a function of carbon consumed, $Y_{12}(t=0) - Y_{12}(t)$. The break in the slope, at $Y_{12}(0) - Y_{12} \approx 2 \times 10^{-3}$, occurs when the heating timescale $t_{\text{H}} = C_P/\varepsilon$ becomes less than the timescale for electron capture onto ^{23}Na , which is ≈ 2700 s at $\rho = 3.0 \times 10^9$ g cm $^{-3}$. We indicate this point with the thin vertical line. To guide the eye, the short dotted line indicates a slope of $\frac{1}{3}$.

As noted by Piro & Bildsten (2008), a one-zone model will overestimate the heat required to raise the central temperature by a given amount, and hence overestimate the amount of ^{12}C that must be consumed during simmering. We perform a calculation similar to theirs: starting with an isothermal white dwarf with a given central density and with a temperature set by equating heating from the $^{12}\text{C} + ^{12}\text{C}$ reaction with neutrino losses, we then raise the central temperature to 8×10^8 K, keeping the total white dwarf mass fixed, and follow an adiabatic temperature gradient until we intersect the

original isotherm at radius r_{conv} , which we then follow to the stellar surface. We compute the total stellar energy, gravitational and thermal, in both cases, and take the difference to find the heat required to raise the central temperature of the star to 8×10^8 K. The temperature of 8×10^8 K is chosen as a fiducial temperature representing the point at which the heating of a fluid element proceeds faster than the convective timescale (Woosley et al. 2004). The evolution of the white dwarf core is not exactly isobaric: the expanding convective zone heats the white dwarf. As the entropy of the white dwarf increases, it expands and reduces the core pressure. For an initial central density $\rho_{\text{init}} = 3.0 \times 10^9$ g cm $^{-3}$, we find that in raising the central temperature from 3×10^8 K to 8×10^8 K the radius expands by a factor of 1.1 and the central pressure decreases to 0.59 of its initial value.

For initial central densities $\rho_{\text{init}} = 10^9$ g cm $^{-3}$, 3×10^9 g cm $^{-3}$, and 6×10^9 g cm $^{-3}$, corresponding to white dwarf masses of $1.35 M_{\odot}$, $1.38 M_{\odot}$, and $1.39 M_{\odot}$, the initial temperatures defined by the onset of thermal instability are 3.8×10^8 K, 1.9×10^8 K, and 1.0×10^8 K, respectively. The energy required to raise the central temperature to 8×10^8 K is $E_c = 2.11$, 4.12, and 5.58 keV per nucleon, respectively. When the central temperature has reached 8×10^8 K, the masses of the convective zone for these three cases are $0.69 M_{\odot}$, $1.10 M_{\odot}$, and $1.29 M_{\odot}$, respectively. The spatial extent of the convective zone, $r_{\text{conv}} \approx 1000$ km for the three cases, is in agreement with the findings of Kuhlen et al. (2006). We checked our computation of E_c by computing $E'_c = \int_{\text{conv.}} C_P [T_{\text{final}} - T_{\text{initial}}] dM$, as was done by Piro & Bildsten (2008). Both methods give comparable estimates, but E'_c slightly underestimates the change in energy (by $\approx 10\%$), because it does not account for the expansion of the white dwarf. Neglecting the change in Y_e as the white dwarf heats introduces a small correction to E_c : for an adiabatic $1.38 M_{\odot}$ white dwarf with a central temperature of 8×10^8 K, a reduction in Y_e by 1.66×10^{-3} reduces E_c by only 3.3%.

If the white dwarf were entirely mixed, raising the central temperature 8×10^8 K would require, for the three ρ_{init} cases here, that $|\Delta Y_{12}| = 1.36 \times 10^{-3}$, 1.66×10^{-3} , and 1.87×10^{-3} , respectively. Because the changes in composition are only mixed over the convective zone, the decrement in Y_{12} , and hence Y_e , is more pronounced there. Using our estimate of r_{conv} , we estimate that within the convective zone $|\Delta Y_{12}| = 3.0 \times 10^{-3}$, 2.1×10^{-3} , and 2.01×10^{-3} , respectively, for $\rho_{\text{init}}/(10^9 \text{ g cm}^{-3}) = 1.0$, 3.0, and 6.0. Should the radial extent of the convective zone be smaller than our estimate, for example because of convective Urca losses (Stein et al. 1999; Stein & Wheeler 2006; Lesaffre et al. 2005), the abundance of ^{12}C will be further reduced in the white dwarf core. A lower ^{12}C abundance reduces the laminar speed of the flame launched at the end of simmering (Timmer & Woosley 1992; Chamulak et al. 2007).

Finally, we estimate at what point the convective mixing timescale becomes shorter than the timescale for electron captures onto ^{23}Na . Using our adiabatic temperature-gradient white dwarf models, we compute the typical convective velocity v_{rms} , and hence a characteristic turnover time $t_{\text{conv}} = r_{\text{conv}}/v_{\text{rms}}$, using the mixing length formalism (see the discussion in Woosley et al. 2004) with the total luminosity and evaluating thermodynamical quantities at their central values. Figure 5 shows t_{conv} (thick lines) for the three cases of ρ_{init} considered above, as well as the electron capture timescale,

t_{ec} for ^{23}Na (thin lines) for those cases with a density above threshold. To estimate the effect of the $^{23}\text{Na}/^{23}\text{Ne}$ pairs on the convective zone, we evaluated the mass fraction of these pairs for the case $\rho_{\text{init}} = 3.0 \times 10^9$ g cm $^{-3}$ when the temperature had risen to $T = 3.5 \times 10^8$ K and $t_{\text{ec}} \approx t_{\text{conv}}$ (Fig. 5, solid line). At this point the convective core has a mass $0.5 M_{\odot}$ which is comparable to their calculation. We estimate, from the energy required to heat the white dwarf to this point, that the mass fraction of $^{23}\text{Na}/^{23}\text{Ne}$ pairs in the convective zone will be $X_{23} = 0.004$ at this time. We note that such a large number of Urca pairs will have a dramatic effect on the properties of the convection zone (Lesaffre et al. 2005). As is evident from Figure 5, there is a range of temperatures for which $t_{\text{conv}} < t_{\text{ec}} < t_{\text{H}}$. In this region, the effective dY_e/dY_{12} will depend on the fraction of mass with densities above the capture threshold and on the effects of Urca losses on the convective flows, but will still be larger than the minimum value set by $^{13}\text{N}(e^-, \nu_e)^{13}\text{C}$. Incorporating the effects of the neutrino luminosity from the $^{23}\text{Na}/^{23}\text{Ne}$ reactions in this regime is numerically challenging (Lesaffre et al. 2005, 2006) and beyond the scope of this work; for now, we just note that this is the primary uncertainty in determining the amount of ^{12}C consumed during the pre-explosive phase, and a better treatment is needed.

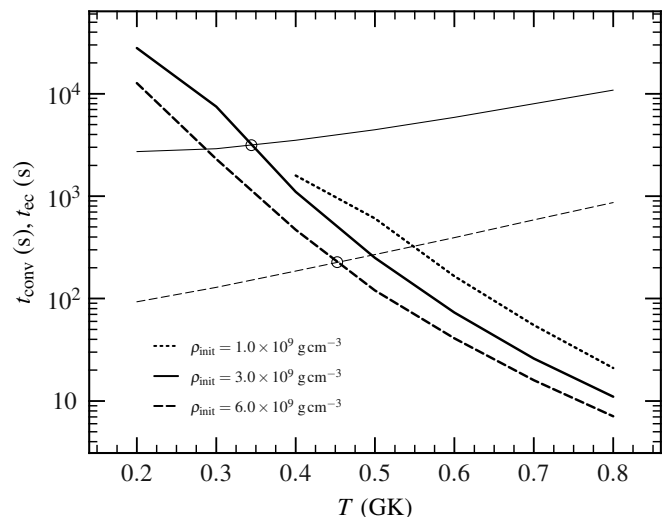


FIG. 5.— Mixing length convective timescales (thick lines) and electron capture timescales (for densities above threshold) for ^{23}Na (thin lines), as a function of the central temperature during the simmering. Three initial densities are shown: 10^9 g cm $^{-3}$ (dotted line), 3×10^9 g cm $^{-3}$ (solid lines), and 6×10^9 g cm $^{-3}$ (dashed lines). The electron capture timescales increase as the white dwarf heats because the density decreases during simmering.

4. DISCUSSION AND CONCLUSIONS

Using a nuclear reaction network coupled to the equation for self-heating at constant pressure (eq. [1]–[2]), we have investigated the change in Y_e induced by electron captures on nuclei produced by ^{12}C fusion during the pre-explosion simmering of the white dwarf. We confirm that there is a maximum Y_e at flame ignition (Piro & Bildsten 2008). We quantified the role of ^{22}Ne and other trace nuclides in setting the change in electron abundance with ^{12}C consumption by using a full reaction network, and we included the heating from electron captures into an excited state of ^{13}C . We gave simple formulae (eq. [5]–[8]) for the energy generation rate, the rate of change in electron abundance, and the rate of change in the

mean atomic mass to include the detailed nuclear physics into large-scale hydrodynamical simulations.

Our estimates of the maximum Y_e at the time of the explosion are roughly similar to those of Piro & Bildsten (2008). If we neglect the effect of thermal neutrino losses on the evolution of the white dwarf, then Y_e is reduced by 2.7×10^{-4} – 6.3×10^{-4} within the convective zone. This reduction in Y_e depends predominantly on the amount of ^{12}C consumed prior to ignition. The electron captures during simmering reduce Y_e below the value set by neutron-rich ^{22}Ne inherited from core He burning by the white dwarf’s progenitor star. Reducing Y_e in the explosion depresses the yield of ^{56}Ni and increases the amount of ^{54}Fe and ^{58}Ni synthesized (Iwamoto et al. 1999; Timmes et al. 2003), even in the absence of further electron captures onto the Fe-peak isotopes in nuclear statistical equilibrium (NSE) in the densest portion of the white dwarf. As a result, any correlation between host system metallicity and white dwarf peak luminosity will be weakened for $Z \lesssim Z_\odot$ (for which the reduction in Y_e due to captures during simmering is greater than the change due to initial white dwarf composition).

To illustrate how the simmering electron captures affect the light curve, we reconstruct the comparison made by Gallagher et al. (2005), who compiled a set of SNe Ia with measured $\Delta m_{15}(B)$, defined as the change in B over 15 days post-peak, and host galaxies with measured abundances of oxygen to hydrogen, denoted O/H. We construct an expression for M_{56} , the mass of ^{56}Ni produced in the explosion, that depends on dY_e/dY_{12} (Table 1), ΔY_{12} , and the host galaxy composition (we assume that the white dwarf has the same O/H ratio as the galaxy). The trace nuclide that predominantly sets Y_e in the white dwarf is ^{22}Ne , which traces the aboriginal abundance of CNO nuclei in the main-sequence star from which the white dwarf evolved. We therefore recast the linear formula for M_{56} (Timmes et al. 2003) in terms of O/H. For simplicity, we fix the $^1\text{H}:$ ^4He ratio, as well as the ratio of heavier elements to ^{16}O , to their solar system values (Asplund et al. 2005) and neglect corrections from the change in [O/Fe] with [Fe/H] (Ramírez et al. 2007) and the increase in [N/O] with [O/H] (Liang et al. 2006). With these assumptions, the mass of ^{56}Ni ejected in the explosion is

$$M_{56} = M_{56,0} \left[1 - 72.7 \left(\frac{\text{O}}{\text{H}} \right) + 58 \frac{dY_e}{dY_{12}} \Delta Y_{12} \right], \quad (9)$$

where $M_{56,0}$ is the total mass of NSE material synthesized at densities where electron captures during the explosion are negligible, dY_e/dY_{12} is the change in electron abundance with carbon consumption given in Table 1, and $-\Delta Y_{12}$ is the total amount of ^{12}C consumed during the pre-explosion convective phase.

Relating this to an observable such as $\Delta m_{15}(B)$ requires an explosion model that follows the radiation transfer. Our interest here is to isolate how M_{56} changes with the CNO abundance of the progenitor when the other parameters, such as the ejecta kinetic energy and the total mass of iron-peak nuclei, are held fixed. This is important, because the relation between light curve width and peak brightness depends on these other parameters as well (see Woosley et al. 2007, for a lucid discussion). We use the model M070103 (Woosley et al. 2007), in which the total mass of iron-peak ejecta is $0.8 M_\odot$: of that, the innermost $0.1 M_\odot$ is stable iron formed *in situ* from electron captures during the explosion, with the remainder being a mix of radioactive ^{56}Ni and stable Fe. Note

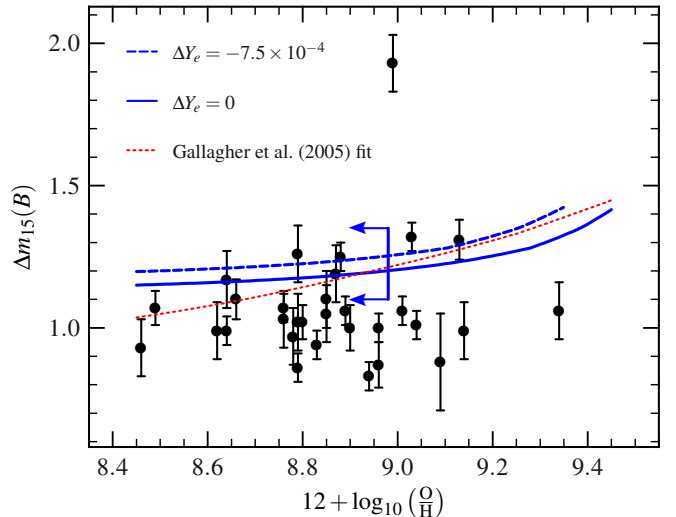


FIG. 6.— Correlation between $12 + \log(\text{O}/\text{H})$ and $\Delta m_{15}(B)$ induced by the electron abundance. The points in the plot are taken from Gallagher et al. (2005). We show the ‘maximal’ case for the reduction in Y_e during simmering (dashed line), in which $dY_e/dY_{12} = 0.30$ in the early stages of the burn, which is an upper limit to the derivative. In this case $\Delta Y_e = -7.5 \times 10^{-4}$. For comparison, we also show the case in which there is no reduction of Y_e during simmering (solid line). Note that the relation between M_{56} and $\Delta m_{15}(B)$ is shallower than that used by Gallagher et al. (2005, dotted line); see the text for an explanation. To the left of the vertical bar, the decrease in M_{56} due to electron captures during simmering will exceed that due to enrichment by ^{22}Ne , and hence any correlation between O/H and $\Delta m_{15}(B)$ will be masked.

that this model follows the peak luminosity-light curve width relation (Phillips 1993), whereas Mazzali & Podsiadlowski (2006) suggest that varying the ratio of ^{56}Ni to stable Fe may create dispersion about this relation.

Using the model of Woosley et al. (2007), we set $M_{56,0} = 0.7 M_\odot$, use equation (9) to compute M_{56} as a function of O/H for different ΔY_{12} , and interpolate from Woosley et al. (2007, Fig. 22) to find $\Delta m_{15}(B)$. Figure 6 displays this result. We plot here a maximal case (dashed line) with $dY_e/dY_{12} = 0.30$ in the initial part of the simmer, appropriate for the one-zone calculation with electron captures onto ^{23}Na (Fig. 4); for this case $\Delta Y_e = -7.5 \times 10^{-4}$. For comparison, we also plot a case (solid line) with $\Delta Y_e = 0$ during simmering. This gives a sense of how large the variation in Y_e might be. The vertical bar indicates the value of $12 + \log_{10}(\text{O}/\text{H})$ at which the change in $\Delta m_{15}(B)$ from the ^{22}Ne abundance equals that from the electron captures during simmering for this maximal case. To the left of this curve the linear correlation between ^{22}Ne abundance and $\Delta m_{15}(B)$ will be masked by variations in the simmering of the white dwarf. For comparison, we also show the data from the compilation of Gallagher et al. (2005) and Hamuy et al. (2000) and plot the relation between $12 + \log(\text{O}/\text{H})$ and $\Delta m_{15}(B)$ used by Gallagher et al. (2005, dotted line). This trend is much steeper than our finding. The difference is due to how the ^{56}Ni mass was varied; whereas the models we use (Woosley et al. 2007) hold the kinetic energy and total mass of iron-peak ejecta fixed, Gallagher et al. (2005) based their peak brightness on delayed detonation models (Höflich et al. 2002) for which a variation in ^{56}Ni also produced a change in the relative amounts of iron-peak and intermediate mass-elements, as well as a different explosion kinetic energy.

It is evident from Fig. 6 that the scatter in the data points is larger than the expected trend due to progenitor composition, especially at sub-solar metallicities. Both ΔY_{12} and

dY_e/dY_{12} depend on the central density, which is not obviously correlated with metallicity, and hence the correlation between peak brightness and O/H will be masked by differences in the pre-explosion simmering. Indeed, if the variation in ΔY_e were as large as the two cases we plot in Fig. 6, then variations in ^{56}Ni would be determined more by ΔY_{12} than by stellar composition for galaxies with sub-solar O/H. There is a general trend that SNe Ia are systematically brighter in galaxies with active star-formation (Hamuy et al. 2000; Gallagher et al. 2005; Sullivan et al. 2006; Howell et al. 2007). Sullivan et al. (2006) showed that the SNe Ia rate increases linearly with the specific star formation rate, and that SNe Ia associated with actively star forming galaxies were intrinsically brighter than those associated with passive galaxies. Although many of these passive galaxies are more massive, and hence more metal-rich (Tremonti et al. 2004), the observed scatter in SNe Ia peak brightnesses remains much larger than the expected trend with metallicity (Piro & Bildsten 2008; D. A. Howell 2007, private communication). This suggests that the correlation with the chemical abundances of the host galaxy is a secondary effect in setting the peak brightness of SNe Ia.

We thank Tony Piro, Lars Bildsten, Andy Howell, and Craig Wheeler for many useful discussions, Francisco Förster and Philipp Podsiadlowski for a detailed comparison of reaction rate networks, Bill Paxton for creating Tioga (available at <http://www.kitp.ucsb.edu/~paxton/tioga.html>), and Michele Berry for assistance with Figure 6. We especially thank Remco Zegers for computing the Gamow-Teller strengths for ^{13}N and the referee for constructive comments. This work was supported by the National Science Foundation, grant AST05-07456, and by the Joint Institute for Nuclear Astrophysics at MSU under NSF-PFC grant PHY02-16783. This research was also supported in part by the NSF under Grant No. PHY05-51164 to the Kavli Institute for Theoretical Physics. Additional support was provided by the U. S. Department of Energy via award KA1401020. Los Alamos National Laboratory is operated by the Los Alamos National Security, LLC for the National Nuclear Security Administration of the U.S. Department of Energy under contract DE-AC52-06NA25396.

REFERENCES

- Ajzenberg-Selove, F. 1991, *Nuclear Physics A*, 523, 1
- Anders, E., & Grevesse, N. 1989, *Geochim. Cosmochim. Acta*, 53, 197
- Asplund, M., Grevesse, N., & Sauval, A. J. 2005, in *Astronomical Society of the Pacific Conference Series*, Vol. 336, *Cosmic Abundances as Records of Stellar Evolution and Nucleosynthesis*, ed. T. G. Barnes, III & F. N. Bash, 25
- Badenes, C., Hughes, J. P., Bravo, E., & Langer, N. 2007, *ApJ*, 662, 472
- Bao, Z. Y., & Kappeler, F. 1987, *At. Data Nucl. Data Tables*, 36, 411
- Becerril Reyes, A. D., Gupta, S., Kratz, K. L., Möller, P., & Schatz, H. 2006, in *Nuclei in the Cosmos IX*, ed. J. Cederkäll et al. (Trieste: SISSA)
- Blondin, S., Dessart, L., Leibundgut, B., Branch, D., Höflich, P., Tonry, J. L., Matheson, T., Foley, R. J., Chornock, R., Filippenko, A. V., Sollerman, J., Spyromilio, J., Kirshner, R. P., Wood-Vasey, W. M., Clocchiatti, A., Aguilera, C., Barris, B., Becker, A. C., Challis, P., Covarrubias, R., Davis, T. M., Garnavich, P., Hicken, M., Jha, S., Krisciunas, K., Li, W., Miceli, A., Miknaitis, G., Pignata, G., Prieto, J. L., Rest, A., Riess, A. G., Salvo, M. E., Schmidt, B. P., Smith, R. C., Stubbs, C. W., & Suntzeff, N. B. 2006, *AJ*, 131, 1648
- Brown, B. A., Etchegoyen, A., Godwin, N. S., Rae, W. D. M., Richter, W. A., Ormand, W. E., Warburton, E. K., Winfield, J. S., Zhao, L., & Zimmerman, C. H. 2004, *OXBASH for Windows*, report 1289, MSU-NSCL
- Busso, M., Gallino, R., & Wasserburg, G. J. 1999, *ARA&A*, 37, 239
- Cameron, A. G. W. 1959, *ApJ*, 130, 429
- Caughtan, G. R., & Fowler, W. A. 1988, *At. Data Nucl. Data Tables*, 40, 283
- Chamulak, D. A., Brown, E. F., & Timmes, F. X. 2007, *ApJ*, 655, L93
- Chou, W.-T., Warburton, E. K., & Brown, B. A. 1993, *Phys. Rev. C*, 47, 163
- Cohen, S., & Kurath, D. 1967, *Nuclear Physics A*, 101, 1
- Feltzing, S., Holmberg, J., & Hurley, J. R. 2001, *A&A*, 377, 911
- Filippenko, A. V. 1997, *ARA&A*, 35, 309
- Fuller, G. M., Fowler, W. A., & Newman, M. J. 1982, *ApJS*, 48, 279
- Gallagher, J. S., Garnavich, P. M., Berlind, P., Challis, P., Jha, S., & Kirshner, R. P. 2005, *ApJ*, 634, 210
- Gallino, R., Arlandini, C., Busso, M., Lugaro, M., Travaglio, C., Straniero, O., Chieffi, A., & Limongi, M. 1998, *ApJ*, 497, 388
- Gamezo, V. N., Khokhlov, A. M., & Oran, E. S. 2004, *Phys. Rev. Lett.*, 92, 211102
- Gasques, L. R., Afanasjev, A. V., Aguilera, E. F., Beard, M., Chamon, L. C., Ring, P., Wiescher, M., & Yakovlev, D. G. 2005, *Phys. Rev. C*, 72, 025806
- Hamuy, M., Trager, S. C., Pinto, P. A., Phillips, M. M., Schommer, R. A., Ivanov, V., & Suntzeff, N. B. 2000, *AJ*, 120, 1479
- Herwig, F. 2005, *ARA&A*, 43, 435
- Hillebrandt, W., & Niemeyer, J. C. 2000, *ARA&A*, 38, 191
- Höflich, P., Gerardy, C. L., Fesen, R. A., & Sakai, S. 2002, *ApJ*, 568, 791
- Howell, D. A., Sullivan, M., Conley, A., & Carlberg, R. 2007, *ApJ*, 667, L37
- Iliadis, C., D’Auria, J. M., Starrfield, S., Thompson, W. J., & Wiescher, M. 2001, *ApJS*, 134, 151
- Iwamoto, K., Brachwitz, F., Nomoto, K., Kishimoto, N., Umeda, H., Hix, W. R., & Thielemann, F. 1999, *ApJS*, 125, 439
- Izzard, R. G., Lugaro, M., Karakas, A. I., Iliadis, C., & van Raai, M. 2007, *A&A*, 466, 641
- Jordan, G. I., Fisher, R., Townsley, D., Calder, A., Graziani, C., Asida, S., Lamb, D., & Truran, J. 2007, *ApJ Letters*, submitted
- Kuhlen, M., Woosley, S. E., & Glatzmaier, G. A. 2006, *ApJ*, 640, 407
- Langanke, K., & Martínez-Pinedo, G. 2001, *At. Data Nucl. Data Tables*, 79, 1
- Lattanzio, J. C., & Boothroyd, A. I. 1997, in *American Institute of Physics Conference Series*, Vol. 402, *American Institute of Physics Conference Series*, ed. T. J. Bernatowicz & E. Zinner, 85
- Leibundgut, B. 2001, *ARA&A*, 39, 67
- Lesaffre, P., Han, Z., Tout, C. A., Podsiadlowski, P., & Martin, R. G. 2006, *MNRAS*, 368, 187
- Lesaffre, P., Podsiadlowski, P., & Tout, C. A. 2005, *MNRAS*, 356, 131
- Liang, Y. C., Yin, S. Y., Hammer, F., Deng, L. C., Flores, H., & Zhang, B. 2006, *ApJ*, 652, 257
- Marion, G. H., Höflich, P., Wheeler, J. C., Robinson, E. L., Gerardy, C. L., & Vacca, W. D. 2006, *ApJ*, 645, 1392
- Marion, J. B., & Fowler, W. A. 1957, *ApJ*, 125, 221
- Mazzali, P. A., & Podsiadlowski, P. 2006, *MNRAS*, 369, L19
- Paczynski, B. 1972, *Astrophys. Lett.*, 11, 53
- Phillips, M. M. 1993, *ApJ*, 413, L105
- Pinto, P. A., & Eastman, R. G. 2000, *ApJ*, 530, 744
- Piro, A. L., & Bildsten, L. 2008, *ApJ*, 673, 1009
- Plewa, T., Calder, A. C., & Lamb, D. Q. 2004, *ApJ*, 612, L37
- Ramírez, I., Allende Prieto, C., & Lambert, D. L. 2007, *A&A*, 465, 271
- Reeves, H., & Salpeter, E. E. 1959, *Physical Review*, 116, 1505
- Rofls, C. E., & Rodney, W. S. 1988, *Cauldrons in the cosmos: Nuclear astrophysics* (Chicago, IL: University of Chicago Press)
- Röpke, F. K., Gieseeler, M., Reinecke, M., Travaglio, C., & Hillebrandt, W. 2006, *A&A*, 453, 203
- Rowland, C., Iliadis, C., Champagne, A. E., Fox, C., José, J., & Runkle, R. 2004, *ApJ*, 615, L37
- Stein, J., Barkat, Z., & Wheeler, J. C. 1999, *ApJ*, 523, 381
- Stein, J., & Wheeler, J. C. 2006, *ApJ*, 643, 1190
- Sullivan, M., Le Borgne, D., Pritchett, C. J., Hodsman, A., Neill, J. D., Howell, D. A., Carlberg, R. G., Astier, P., Aubourg, E., Balam, D., Basa, S., Conley, A., Fabbro, S., Fouchez, D., Guy, J., Hook, I., Pain, R., Palanque-Delabrouille, N., Perrett, K., Regnault, N., Rich, J., Taitel, R., Baumont, S., Bronder, J., Ellis, R. S., Filiol, M., Lusser, V., Perlmutter, S., Riposte, P., & Tao, C. 2006, *ApJ*, 648, 868
- Timmes, F. X., Brown, E. F., & Truran, J. W. 2003, *ApJ*, 590, L83
- Timmes, F. X., & Woosley, S. E. 1992, *ApJ*, 396, 649

- Tremonti, C. A., Heckman, T. M., Kauffmann, G., Brinchmann, J., Charlot, S., White, S. D. M., Seibert, M., Peng, E. W., Schlegel, D. J., Uomoto, A., Fukugita, M., & Brinkmann, J. 2004, *ApJ*, 613, 898
- Wosley, S. E., Kasen, D., Blinnikov, S., & Sorokina, E. 2007, *ApJ*, 662, 487
- Wosley, S. E., Wunsch, S., & Kuhlen, M. 2004, *ApJ*, 607, 921
- Yakovlev, D. G., Gasques, L. R., Afanasjev, A. V., Beard, M., & Wiescher, M. 2006, *Phys. Rev. C*, 74, 035803
- Zegers, R. G. T., Brown, E. F., Akimune, H., Austin, S. M., van den Berg, A. M., Brown, B. A., Chamulak, D. A., Fujita, Y., Galès, S., Harakeh, M. N., Hashimoto, H., Hayami, R., Hitt, G. W., Itoh, M., Kawabata, T., Kawase, K., Kinoshita, M., Nakanishi, K., Nakayama, S., Okamura, S., Shimbara, Y., Uchida, M., Ueno, H., Yamagata, T., & Yosoi, M. 2007, *Phys. Rev. C*, submitted